# Fretting wear modeling of 3D and 2D Hertzian contacts with a third-body layer using a Winkler elastic foundation model

Simon Garcin, Soha Baydoun, Pierre Arnaud, Siegfried Fouvry

# Fretting wear modeling of 3D and 2D Hertzian contacts with a third-body layer using a Winkler elastic foundation model

Simon Garcin[a]*, Soha Baydoun[a*], Pierre Arnaud[b*], Siegfried Fouvry[a*]

[a]Ecole Centrale de Lyon, LTDS Laboratory, 36 av Guy de Collongue, 69130 Ecully, France

[b]MINES ParisTech, Centre des Matériaux, 63-65 rue Henri-Auguste Desbrueres, F-91003 Évry cedex, France

*Corresponding authors email addresses: soha.baydoun@ec-lyon.fr (S. Baydoun), s.a.r.garcin@gmail.com (S. Garcin), pierre.arnaud@mines-paristech.fr (P. Arnaud) and siegfried.fouvry@ec-lyon.fr (S. Fouvry)

## Abstract

This article aims at modeling fretting wear in a 2D cylinder-on-flat contact using Winkler elastic foundation model (WK). This model is compared with existing FEM and semi-analytic approaches as well as with experiments where the potentials and limits of the latter are carefully discussed. Following this, WK approach is extended to a 3D sphere-on-flat contact where the results showed that this approach captures nicely the 3D experimental wear profile with lower computation costs compared to semi-analytic approach. Finally, WK approach is applied for more complex cases as reciprocating sliding and fretting wear incorporating a third body layer in both 2D and 3D configurations. Interesting results were obtained confirming the potential of this approach to model complex sliding and geometrical conditions.

**Keywords:** Semi-analytic wear model; Winkler elastic foundation model; 2D and 3D Hertzian contact; Fretting wear.

## 1. Introduction

The prediction and simulation of wear volume extension from fretting to reciprocating sliding conditions were extensively addressed during the past decades. Various strategies based on Archard theory, friction energy approach, and Third Body Theory (TBT) were implemented providing pertinent predictions as long as the wear

parameters (i.e. Archard wear coefficient or friction energy coefficient) used for the predictions are estimated from representative tribological contact pressure, sliding amplitude and ambient conditions [1–6]. However, the main objective of industrial design strategies consists in predicting the maximum wear depth in fretted interfaces which implies to shift from a global wear volume description to a local wear depth prediction. Such local analysis requires numerical simulations to compute local Archard or friction density taking into account the continuous evolution of contact geometry induced by the surface wear process. Various incremental numerical approaches can be considered like Finite Element Method (FEM) [7–11], Discrete element modeling [12,13] or Semi-Analytic approaches (SA) [14–16] which incorporate the effect of different wear mechanisms including abrasion, adhesion as well as third body flows. FEM approaches are useful and can be adapted to any contact assembly but they are rather slow and require huge computation capacities especially for 3D contact situations. Alternatively the SA approaches are generally restricted to a reduced range of applications, but can provide a very precise solution for a much lower computational cost.

In this article, an alternative Winkler approach (WK) will be investigated. This approach, which is originally used in geotechnical and structural foundation designs in which the soil is represented as linear vertical springs supporting the foundation, is transposed to tribological and wear analysis by several authors [17–19]. It provides very good wear prediction with a relative error less than 5% compared to reference SA or FEM simulations. Additionally, WK approach can be adapted to any contact configuration like the FEM providing a lower computation cost compared to SA and FEM approaches.

One limitation of the Winkler approach (WK) is the difficulty to establish the incipient contact pressure conditions [20]. However, interesting results have been obtained for

long term surface wear extension when the effect of initial contact conditions are progressively erased by the running in wear process [17,21,22]. The purpose of this research work is to deepen the capacity of the WK approach to predict 2D cylinder-on-flat but also 3D sphere-on-flat surface wears profiles. The analysis will compare the evolution of the maximum wear depth predictions between WK and reference SA simulations. Limits and advantages of the WK approach will be discussed taking into account the computation time and the capacity to be transposed to more complex 3D contact configurations like pin-on-disk situations.

## 2. Description of the Winkler wear model

The wear model developed in this article solves the mechanical problem using the Winkler elastic foundation model [20]. The formulation is expressed for a 3D $(x, y)$ surface where x axis is related to the sliding direction and y axis to the transverse direction. The wear depth evolution is related to the z direction. Note that an equivalent 2D contact configuration is achieved by removing the "y" variable from the following relationships. Both the contact surfaces of the plane surface and the counter body are respectively described by the variables $(x_p, y_p, z_p)$ and $(x_c, y_{c,} z_c)$. The spatial discretization step size is denoted by $\lambda$. The wear process is simulated by realizing a specific number $N_{cycles}$ alternated (i.e. fretting) sliding cycles, and by applying after each sliding cycle a local wear increment of the surface profiles. This consists in shifting both the plane $(x_p, y_p, z_p)$ and the counterpart $(x_c, y_{c,} z_c)$ profiles to simulate the local increment of wear depth removed from the bulk fretted surfaces. A friction energy approach [11,23,24] is considered which implies that the local increment wear depth Δz is assumed proportional to the local friction energy density dissipated at the x position of the fretted contact during the numerical cycle. Dealing with the gross slip regime, a perfect sliding assumption is made to simplify the

tangential and sliding problems. This assumption allows reducing the complexity of the problem to solve, but it restrains the range of possible applications by excluding the partial slip problems.

### 2.1. Resolution of the contact problem

The Winkler model considers a series of independent springs as described in Fig.1. To generate a contact force, a prescribed vertical displacement $\delta_z$ is applied to the moving part. It leads to a modification of the relative positions of the parts, which is formalized by the $g(x, \delta_z)$ function:

$$g(x, y, \delta_z) = h(x, y) - \delta_z = z_c(x, y) - z_p(x, y) - \delta_z \quad (1)$$

The interpenetration of the two rigid surfaces is thus measurable ($g(x, y, \delta_z) \leq 0$). From this data, the local pressure $p(x, y, \delta_z)$ is estimated solving Eq. 2, with $K$ being the stiffness of the springs:

$$p(x, y, \delta_z) = \begin{cases} -\frac{K}{\lambda} \times g(x, y, \delta_z) & \text{if } g(x, y, \delta_z) \leq 0 \\ 0 & \text{if } g(x, y, \delta_z) > 0 \end{cases} \quad (2)$$

The normal load is evaluated by integrating the pressure profile (Eq. 3) so that it corresponds to the applied normal force. For instance, using the Matlab “fsolve” function, the solution displacement leading to the desired normal load can be easily achieved. The function to be solved is given in Eq. 4, and the solution which is the normal displacement is denoted by $\delta_{z\,sol}$.

$$P(\delta_z) = \iint p(x, y, \delta_z) dx.dy \quad (3)$$

$$P(\delta_{z\,sol}) - P_N = 0 \quad (4)$$

The given procedure is applied for a given x position. To fully describe a gross slip fretting cycle, the procedure is repeated at different x increments defining the fretting

or reciprocating sliding path. Then, by using the perfect sliding assumption, the tangential mechanical problem is solved thanks to the coulomb law:

$$q(x) = \mu \times p(x,y) = \mu \times p(x,y,\delta_{z\,sol}) \tag{5}$$

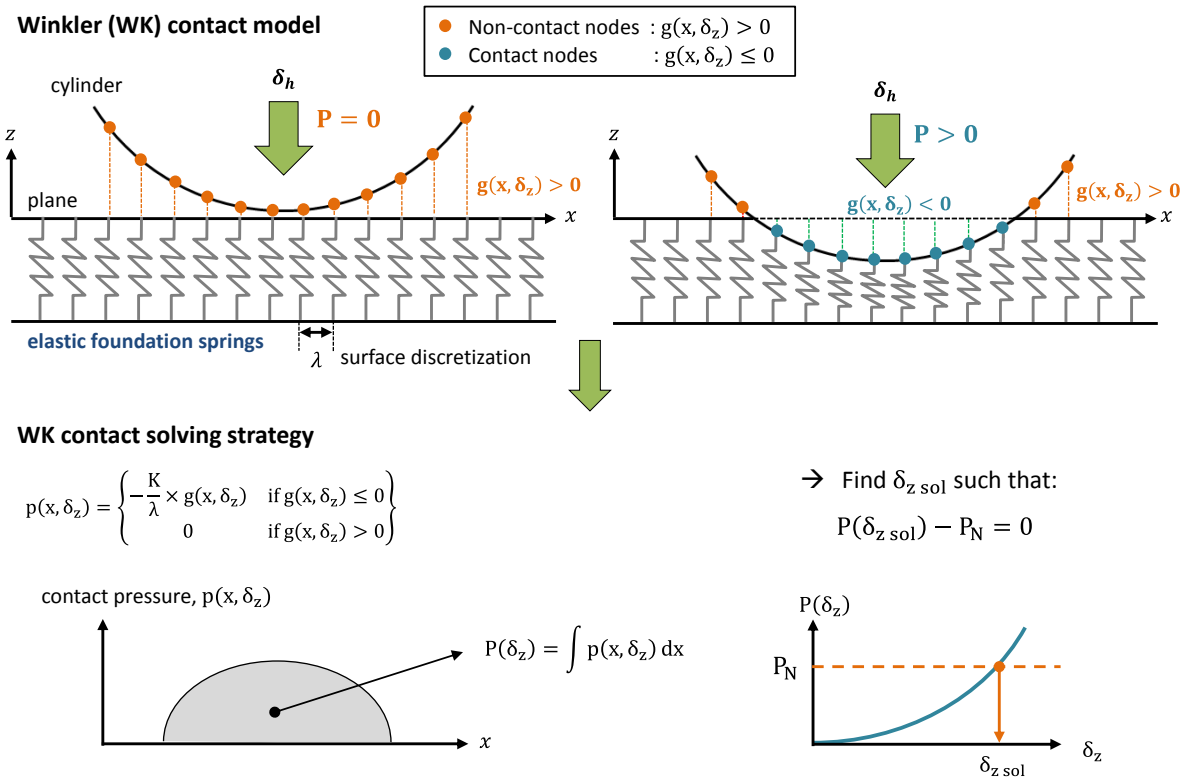


**Fig.1.** (a) Illustration of the Winkler contact model for a 2D cylinder-on-flat contact configuration (counterpart=cylinder, neglecting "y" transverse direction); (b) Illustration of the strategy to establish the contact pressure profile.

## 2.2. Description of the friction energy density simulation

To simulate wear, the friction energy approach is considered expressing the surface wear volume (V) as a linear function of the interfacial shear work (i.e. friction energy ∑Ed) using the so-called energy wear coefficient (α) such that V= α∑Ed [4]. Such global approach can be derived at local scale so that wear depth h(x,y) is proportional to the cumulated friction energy density $\sum \varphi(x,y)$ dissipated at a point M(x,y) [23] such that:

$$h(x,y) = \alpha \sum \varphi(x,y). \tag{6}$$

As illustrated in Fig. 2, the simulation of an alternated (i.e. fretting or reciprocating) cycle consists in imposing a succession of small tangential sliding increments $\Delta s$ for each of them to solve the former contact procedure thus to extract the corresponding incremental pressure and shear profiles. Assuming two successive increments i and i+1, the $i^{th}$ increment of friction work density of the $j^{th}$ fretting cycle is given by:

$$\varphi_{j,i}(x,y) = \frac{q_i(x,y)+q_{i+1}(x,y)}{2} \times \Delta s \quad (7)$$

Where $q_i(x,y)$ and $q_{i+1}(x,y)$ are surface the shear profiles at the sliding increment i and i+1.

The simulation of a single fretting cycle is composed of $N_{itv}$ sliding increments, so the fretting energy density introduced at the M(x,y) position of a 3D contact during a $j^{th}$ fretting cycle is obtained by summing the contribution of each sliding increment so that :

$$\varphi_j(x,y) = \sum_{i=1}^{N_{itv}} \varphi_{j,i}(x,y) \quad (8)$$

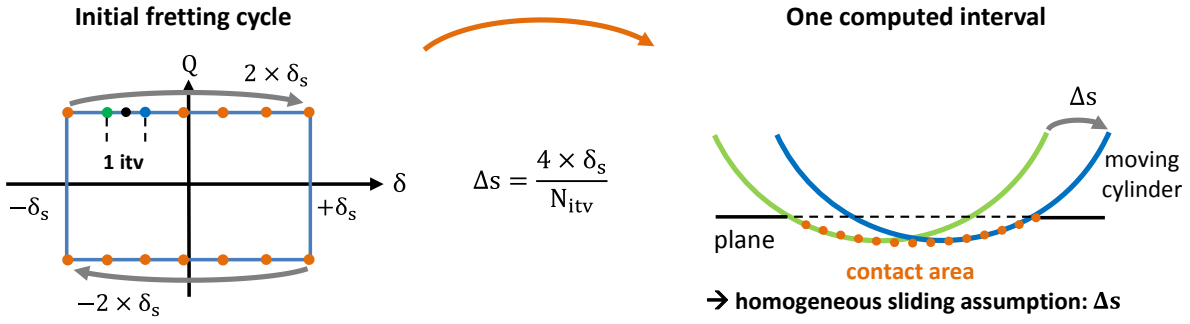


**Fig. 2.** Description of the incremental description of the sliding contact: after each Δs sliding increment expressed as a function of the sliding amplitude $\delta_s$ and the number of iterations during the alternated sliding cycle ($N_{itv}$), the WK contact algorithm is applied to extract the corresponding pressure profile and the related increment friction of friction energy density.

Note that for alternated sliding condition like gross slip fretting, the back and forth motion of the contact implies that the sliding increment can be expressed as a function of the sliding amplitude $\delta_s$ such that:

$$\Delta s = \frac{4 \times \delta_s}{N_{itv}} \quad (9)$$

Finally, the accumulated friction energy $\varphi(x,y)$ over the whole fretting test is derived by summing the contribution of each fretting cycles such that:

$$\varphi(x,y) = \sum_{j=1}^{N} \varphi_j(x,y) \quad (10)$$

With N being the total number of (experimental) fretting cycle.

The computation of each experimental fretting cycle is quite tricky and could be very long. In reality the surface wear evolution is rather slow so that the friction energy density profile may be assumed constant during few tens of cycles. Therefore a β acceleration factor is introduced which corresponds to number of experimental fretting cycles simulated during each numerical fretting cycle.

The accumulated friction energy density is therefore computed by summing the contribution of each numerical cycle so that:

$$\varphi(x,y) = \sum_{j=1}^{N_{num}} \beta_j \times \varphi_j(x,y) \text{ with } N = \sum_{j=1}^{N_{num}} \beta_j \quad (11)$$

where $N_{num}$ is the number of numerical fretting cycles required to simulate the N experimental fretting cycles. The acceleration factor can be constant $(i.e.\ \beta_j = \beta)$ or expressed as an increasing function of the wear depth extension. Small $\beta_j$ values are applied at the beginning of the computation to better describe the fast evolution of the contact geometry at the beginning whereas larger $\beta_j$ values are considered during the steady state wear regime when lower and quasi flat contact pressure profiles are achieved. Assuming the friction energy wear volume formulation:

$$V = \alpha \times \Sigma E d \quad (12)$$

Supposing continuity from global to local wear process, the increment of wear depth $\Delta h_j(x,y)$ generated during a $j^{th}$ numerical fretting cycle can be estimated using the following expression (Fig. 3):

$$\Delta h_j(x,y) = \alpha \times \beta \times \varphi_j(x,y) \tag{13}$$

The total wear depth is computed by summing the contribution of each numerical cycle:

$$h(x,y) = \alpha \times \sum_{j=1}^{N_{num}} \left[ \beta \times \varphi_j(x,y) \right] \tag{14}$$

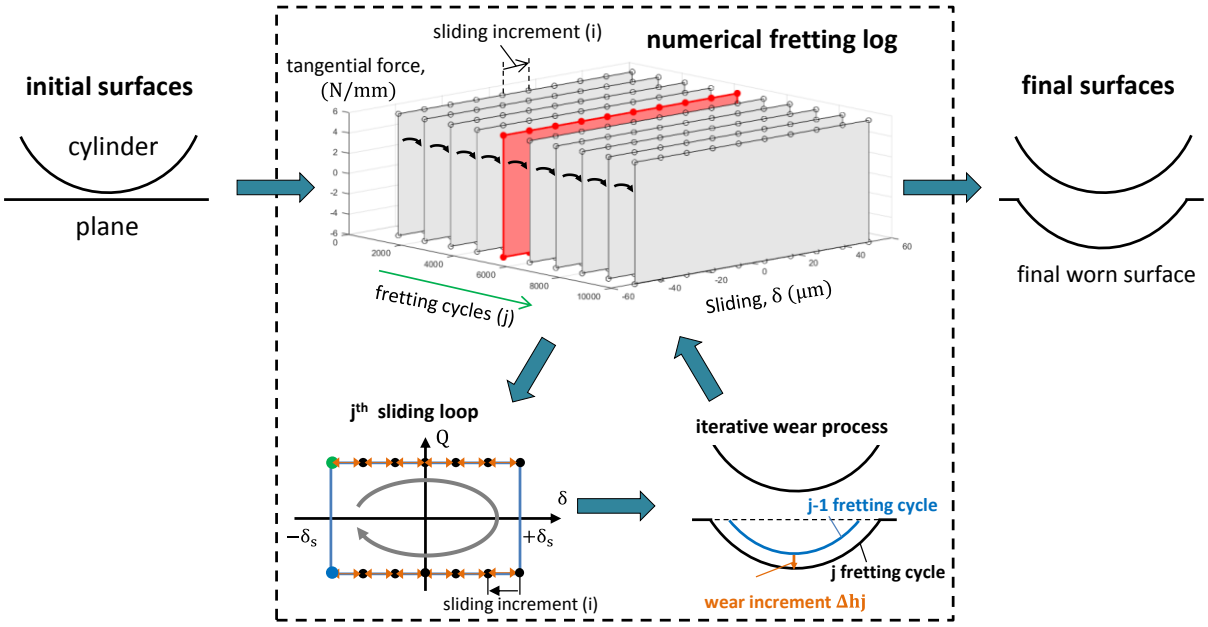


**Fig. 3.** Illustration of the fretting log (accumulated fretting cycles) and the related surface wear profile evolution (2D cylinder-on-flat contact).

Note that after each $j^{th}$ numerical cycle the surface profile of the contacted counter parts are updated in order to remove the worn thickness. To simplify the description we assume that only the plane surface is worn:

$$y_{p,j}(x,y) = y_{p,j-1}(x,y) - \Delta h_j(x,y) \tag{15}$$

Fig. 4 illustrates the global computation algorithm for a 2D contact configuration. It mainly consists in two main loops and a central brick related to the contact solver ("Load resolution"). Fig. 4 illustrates the computation process and the related wear profile evolution.

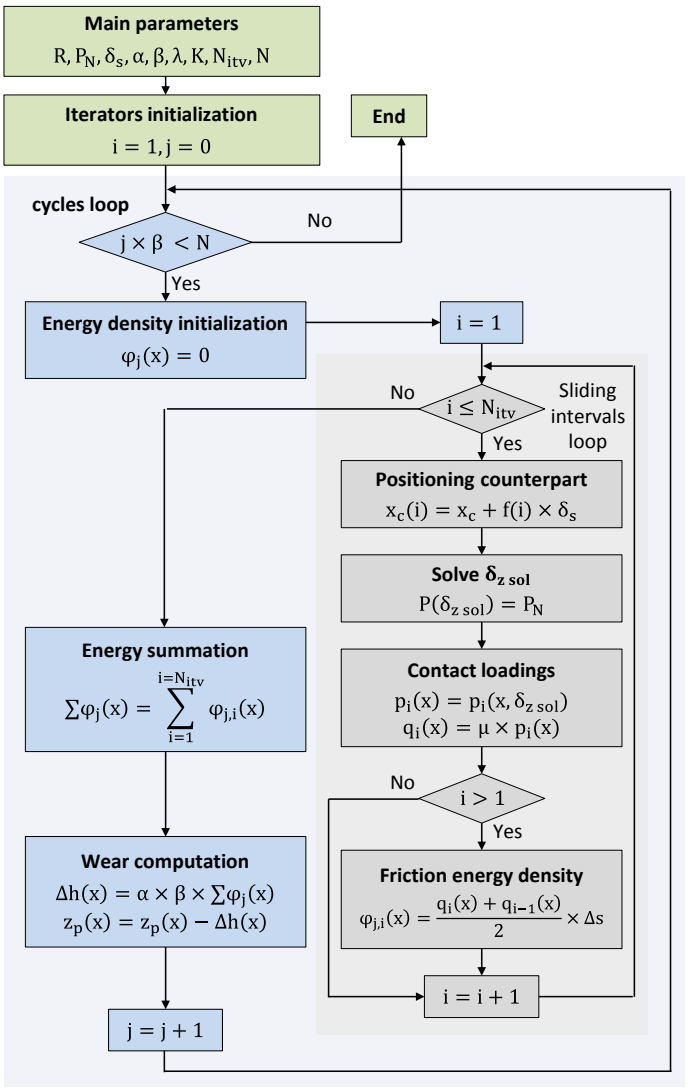


**Fig. 4.** Illustration of the Winkler wear model algorithm for a 2D contact configuration (i.e. neglecting the y transverse direction).

## 2.3. Identification of the Winkler stiffness parameter from Hertzian theory

In contrast to FEM and SA numerical simulations which precisely solve the contact problem taking into account surface and subsurface deformations, the WK approach considers a simplified approach where the contact area and the contact pressure profile are established from a single spring layer deformation. This assumption allows very fast computations but misestimates the exact pressure profiles in particular for non-conformal contact pressure profiles like Hertzian cylinder-on-flat or sphere-on-flat configurations. It will be shown successively that this error is drastically reduced

when the pressure profile converges toward a flat distribution with surface wear extension.

A key aspect of the WK model concerns the estimation of a representative spring "pressure" stiffness parameter $K$ marking the link between the elastic properties of the materials and the contact mechanics response. K.L Johnson suggests an analytical formulation expressing the "pressure" stiffness parameter so that for a given normal force $P_N$, the WK contact radius is similar to the reference Hertzian value (i.e. $a_{WK} = a_H$). Focusing on a 2D cylinder-on-flat contact configuration it leads to the following relationships:

$$K\,(\mathrm{MPa.mm^{-1}}) = 1.18 \times \frac{E^*}{a_H} \tag{16}$$

$$\text{with } E^* = \left(\frac{(1-\nu_p{}^2)}{E_p} + \frac{(1-\nu_c{}^2)}{E_c}\right)^{-1} \quad \text{and} \quad a_H = \left(\frac{4\times P_N \times R}{\pi E^*}\right)^{\frac{1}{2}} \tag{17}$$

$$\text{where } p_{0,H} = \left(\frac{P_N \times E^*}{\pi R}\right)^{\frac{1}{2}} \text{ and } p_H(x) = p_{0,H} \times \left(1 - \frac{x^2}{a_H^2}\right)^{\frac{1}{2}} \tag{18}$$

with $E_p$, $E_c$ and $\nu_p$, $\nu_c$ are the Young's modulus and Poisson's ratios of the plane the counterpart respectively, $P_N$ is the applied (i.e. Nominal) linear normal force and $R$ is the cylinder radius. The K parameter is function of the Hertzian contact radius $a_H$ and therefore depends on the elastic properties of the material but also on the cylinder radius and the applied normal load.

On the other hand, for sphere-on-flat the elastic Hertzian contact parameters are expressed by the following relationships:

$$a_H = \left(\frac{3\times P\times R}{4E^*}\right)^{\frac{1}{3}} \tag{19}$$

$$p_{0,H} = \frac{3\times P}{2\times\pi\times a_H^2} = p_{0,H} = \left(\frac{P\times E^*}{\pi R}\right)^{\frac{1}{2}} \tag{20}$$

$$p(x) = p_{0,H} \times \left(1 - \frac{r^2}{a_H^2}\right)^{\frac{1}{2}} \text{ with } r^2 = x^2 + y^2 \quad (21)$$

$$K\,(\mathrm{MPa.mm^{-1}}) = 1.70 \times \frac{E^*}{a_H} \quad (22)$$

Although the Winkler stiffness parameter "K" is determined from the initial intact geometry defined by the Hertzian theory, it can be used in modelling the contact interaction even when the contact geometry changes during fretting wear extension. This insensitivity to elastic stiffness can be explained by the fact that when the surface wears out, the contact passes gradually from a Hertzian to a conformal contact, at least at the contact interface. It is this conforming zone which provides this insensitivity to the elastic stiffness. Besides, Argatov and co-authors revealed analytically, through asymptotic modeling of reciprocating sliding wear, a weak effect of elasticity on surface wear [25–27]. Based on this, it seems relevant to apply constant contact stiffness along the simulation which will be more effective especially at large number of cycles where the interface converges to conformal configuration.

## 3. Semi-Analytic wear model

The Semi-Analytic wear model (SA) uses exactly the same algorithm (Fig. 4) except that the contact solving subroutine (i.e. contact pressure profile computation) is achieved using the Gallego et al. formalism [14,28,29].

## 4. Comparison between WK and SA for a 2D cylinder-on-flat contact.

To check the performance of WK approach, the latter is compared with SA and FEM models for a cylinder-on-flat steel contact configuration whose elastic properties and wear parameters are compiled in Table 1 [30]. Assuming reference test conditions consisting of a linear normal force P=10 N/mm and a sliding amplitude $\delta_s$=±8 µm, it was found that $p_{0,H}$ = 269 MPa, $a_H$ = 23.7 µm, K = 5.47x10$^6$ MPa/mm.

**Table 1.** Elastic properties and wear parameters used to simulate cylinder-on-flat wear profiles of 316L/304L steel interface [30].

| Elastic modulus, $E_p$=$E_c$ (GPa) | Poisson's coefficient, $v_c$= $v_p$ | Cylinder radius, R (mm) | Friction coefficient | Wear coef. $\alpha_p$ ($mm^3/J$) [30] | Wear coef. $\alpha_c$ ($mm^3/J$) [30] |
|---|---|---|---|---|---|
| 200 | 0.3 | 4.85 | 0.6 | $7.7\ 10^{-6}$ | 0 |

### 4.1. Prediction of the Hertzian contact pressure

Fig. 5 compares the WK pressure profile obtained using the K.L Johnson's approximation versus the Hertzian reference. As expected, the Winkler contact radius ($a_{WK}$) is coherent with the Hertzian contact radius, but the pressure profiles are very different which underlines the limitation of the Winkler model to correctly describe the initial contact pressure distribution as this simplified approach does not solve the global contact interface and more particularly the subsurface elastic deformation. However, WK model provides a more elongated pressure distribution ($p_{0,WK}$= 316 MPa) compared to the reference Hertzian profile. On the other hand, SA approach displays a perfect superposition with Hertzian simulations. This confirms that SA modeling, which is more complex to implement and requires longer simulations, provides exact estimation of the contact pressure field and therefore will be considered as the reference to compare the alternative "low cost" WK strategy.

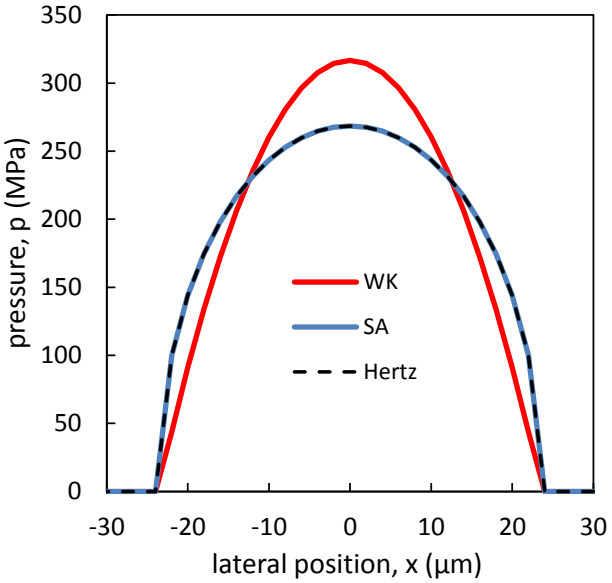


**Fig. 5.** Comparison between explicit Hertzian pressure profile and the pressure profiles given by WK and SA numerical computations at the first indentation stage (i.e. without surface wear simulation, N=0) (elastic cylinder-on-flat contact: Table 1, P = 10 N/mm).

### 4.2. Effect of the fretting loading parameters

A set of surface wear simulations was performed to compare both WK and SA contact solving strategies for a given 2D cylinder-on-flat contact configuration. Different aspects such as the test duration, the sliding amplitude, the normal force and contact radius effects were investigated. The constant parameters are the elastic modulus (E) and Poisson's ratio (v) of the two homogeneous steel counterparts, the friction coefficient (μ) and the energy wear coefficient (α). These different data are compiled in Table 1.

The other variables required by the simulation are the spatial discretization (λ), the number numerical steps during a fretting cycle ($N_{itv}$), the linear normal force (P), the sliding amplitude ($\delta_s$), the cylinder radius (R),the acceleration factor (β) and the total number of fretting cycles simulated (N). Similar values will be applied for each WK and SA simulation to ensure reliable comparisons. To quantify the performance of the WK simulations a maximum wear depth error indicator is considered:

$$\%E_{h,WK} = 100 \times \frac{h_{WK} - h_{SA}}{h_{SA}} \quad (23)$$

With $h_{SA}$ the maximum wear depth given by the reference SA simulation and $h_{WK}$ the maximum wear depth obtained by the WK computation assuming similar loading conditions. The lower the $\%E_{h,WK}$ indicator, the better is the prediction given by the WK model.

#### 4.2.1. Effect of test duration

Fig. 6 compares two wear profiles given by SA and SW computations for a similar set of loading conditions (Table 1) for $\delta_s$=±8 µm, $P_N$=10 N/mm. By increasing the test duration from N=100 to 10000 cycles, the error indicator decreased significantly from $\%E_{h,WK}$ = 16.2% to 2.5% respectively (Fig. 6a &b). Indeed, at low number of fretting cycles, WK approach, by overestimating the peak pressure, overestimates the maximum wear depth and underestimates the lateral contact extension. Hence, it leads to a conservative maximum wear depth prediction satisfying the usual industrial requirements for a safe fretting wear design.

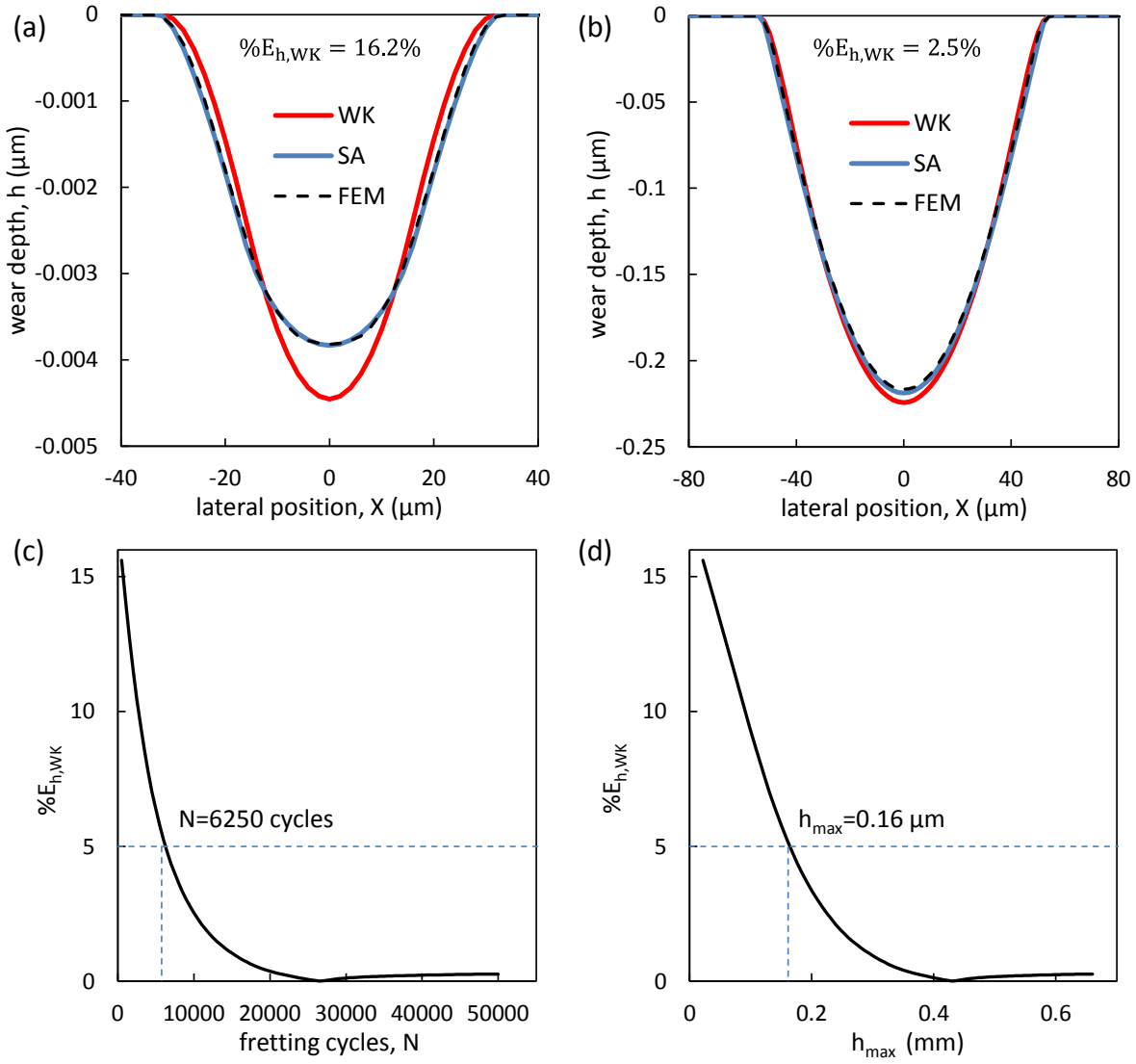


**Fig. 6.** Comparison between SA, WK and FEM worn profiles for (a) N=100 cycles and β=20 and (b) N=10000 cycles and β=200 ($\delta_s$=±8 µm, $P_N$=10 N/mm, material and loading parameters are shown in Table 1). Evolution of the index error $\%E_{h,WK}$ with respect to the (c) number of fretting cycles and (d) maximum wear depth $h_{max}$.

Even though the relative error at N=100 cycles $\%E_{h,WK}$ = 16.2% is quite significant, this value must be related to maximum wear depth less 0.045 µm which is insignificant regarding most of the fretting wear analysis. The $\%E_{h,WK}$ error index decreases below a threshold $\%E_{h,WK,th}$=5% after 6500 fretting cycles which still corresponds to a quasi-negligible 0.16 µm wear depth for the simulated R=4.85 mm 316L/304L steel interface (Fig. 6c &d). Then, the index error stabilizes around 0.25 % around 50000 cycles. Most the fretting wear investigations concerns wear depth

deeper than 1 µm. This result confirms that despite its lack of efficiency to simulate unworn Hertzian contact, the Winkler model appears as a pertinent strategy to predict the wear profiles of classical fretting wear investigations. Indeed, as previously demonstrated, surface wear process changes the initial Hertzian pressure toward a flat distribution in very few cycles which can explain the sharp reduction of the $\%E_{h,WK}$ index error and the potential interest to apply a WK contact solving approach to simulate surface wear process.

Although SA simulations provide exact pressure profile (Fig. 5), it is necessary to validate the surface wear algorithm (Fig. 4). This can be done by comparing the worn profiles given by SA contact analysis combined with the given surface wear algorithm versus a well-established FEM wear modeling (Wear Box) previously detailed in [11,23,24]. Applying similar loading conditions, the relative error between the proposed surface wear algorithms combined with SA contact solving and the FEM simulations falls below 1% (Fig. 6a &b). This confirms the given surface wear-SA model as a reliable reference to compare the alternative WK contact solving approach.

Table 2 compares the computation time required for each numerical strategy SA, WK and FEM. While the $\%E_{h,WK}$ falls below 1%, the WK is nearly 3 times faster than the equivalent SA analysis but more than 300 times faster than the FEM computations. This analysis confirms the capacity of semi-analytical computations (SW & SA) to simulate worn profiles in a faster way than FEM strategy.

**Table 2.** Computation time of the different models on the reference simulation (Fig. 6b, Table 1, N=10000 cycles, β=200, $\delta_s$=±8 µm, $P_N$=10 N/mm).

| Model | Computation time |
|---|---|
| WK | 25 sec |
| SA | 1min 8sec |
| FEM | 2h 11min |

### 4.2.2. Effect of loading parameters

The effect of the sliding amplitude, normal force and cylinder radius are investigated regarding the surface wear evolution (Fig. 7) keeping constant the material and contact geometry parameters compiled in Table 1. By maintaining P=10 N/mm but varying the sliding amplitude from 5 to 10 µm, the $\%E_{h,WK}$ error decreases earlier below 5% at 4000 cycles for $\delta_s$= 5 µm and 14000 cycles for $\delta_s$=10 µm. The decrease of the $\%E_{h,WK}$ is a function of the surface damage and wear volume. Hence, the larger is the sliding amplitude, the larger the surface wear extension, and the lower the $\%E_{h,WK}$. Opposite tendency is observed when the contact radius and /or the cylinder radius are increased as increasing the latter increases the number of cycles required for decreasing $\%E_{h,WK}$ below 5%. This comes from the fact that WK approach is less precise concerning contact pressure computation that the SA which directly affects the wear profile estimation while varying the normal force and the contact radius. To interpret this tendency for the normal force for instance, it must be underlined that an increase in the normal force promotes a rising of the slope of the pressure profile but also an extension of the contact radius. For instance assuming Hertzian hypothesis, an increase in the normal load from P=10 N/mm to P=20 N/mm increases the maximum pressure from $p_{0,H}$ =269 to 380 MPa and extends the Hertzian contact radius from $a_H$= 23.7 to 33.5 µm. Taking into account the conclusions derived from the sliding amplitude analysis, it can be understood why larger and sharper pressure profiles, by inducing higher fluctuations of the friction energy density as a function of the contact stress analysis, can increase the $\%E_{h,WK}$ with the applied normal load. However, it must be underlined the very small wear depth below which the $\%E_{h,WK}$ error is significant. Based on Fig. 7, we can conclude that the error of wear depth prediction falls below 5% when the wear depth is deeper than 1 µm which corresponds to less than 4 % of the initial Hertzian contact radius.

This value is very small compared to the common fretting wear depth investigations which are usually deeper than 5 to 10 µm. Hence, this suggests that the WK surface modeling appears as a consistent numerical strategy to simulate the wear profiles for most of the fretting wear applications.

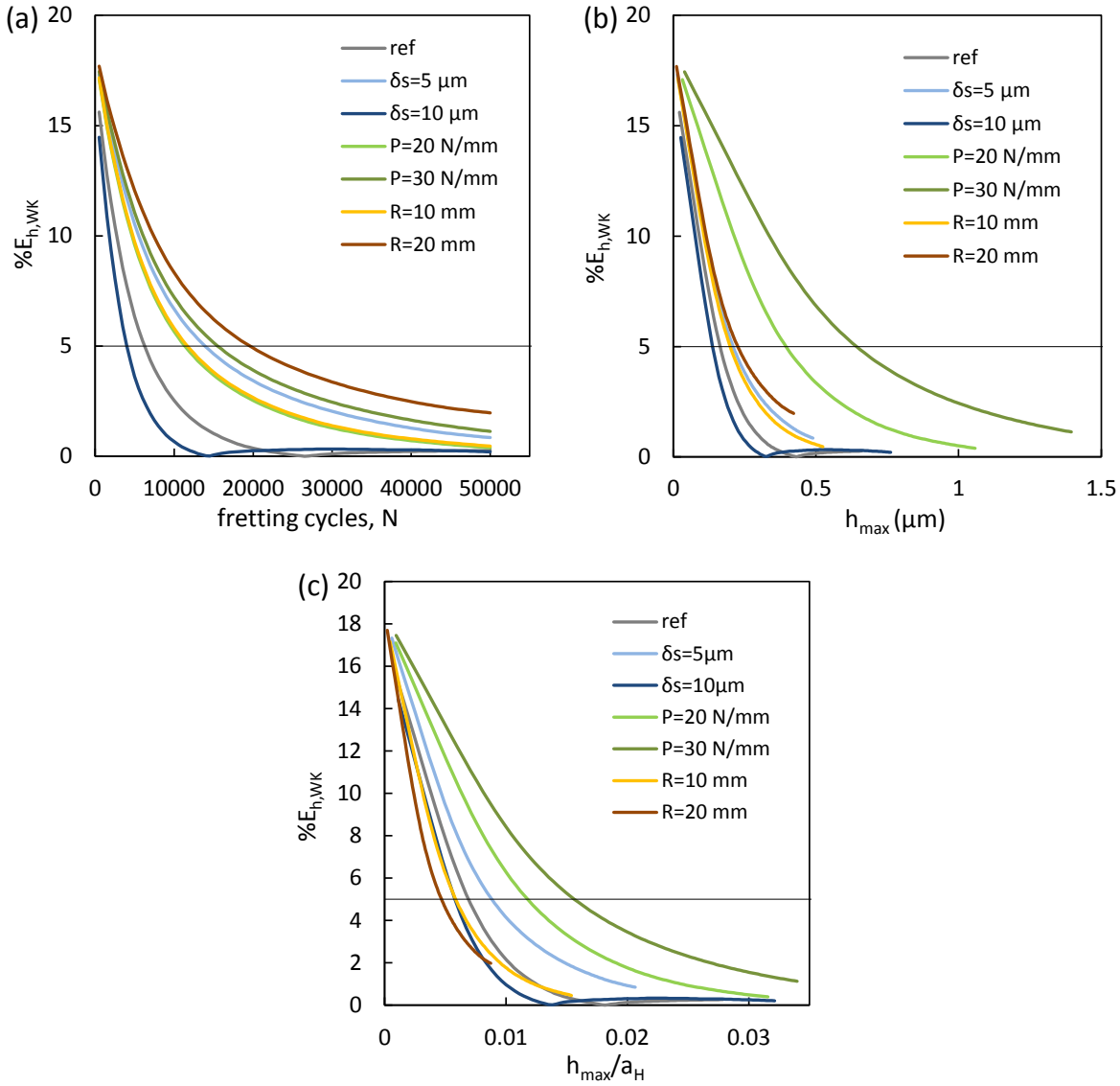


**Fig. 7.** Evolution of the index error $\%E_{h,WK}$ with respect to the (a) number of fretting cycles and (d) maximum wear depth $h_{max}$; (c) with maximum wear depth normalized by the initial Hertzian contact size ($h_{max}/a_H$).

## 5. 3D surface wear simulations

### 5.1. Description of the contact geometry and wear models

An equivalent 3D sphere-on-flat contact configuration is implemented (Fig. 8a). Compared to the former 2D algorithm, the numerical strategy consists of solving the

contact pressure distribution along the x axial and y the transverse directions. The wear algorithm is also adapted to compute the 3D evolution of the surface wear profile along X but also the Y directions. Fig. 8b &c illustrate the 3D surface wear evolution of a fretting sphere-on-flat contact configuration for different fretting cycles and the estimation of the maximum wear depth at y=0 ($h_{max}=\max|z_p(x_p,y_p)|$).

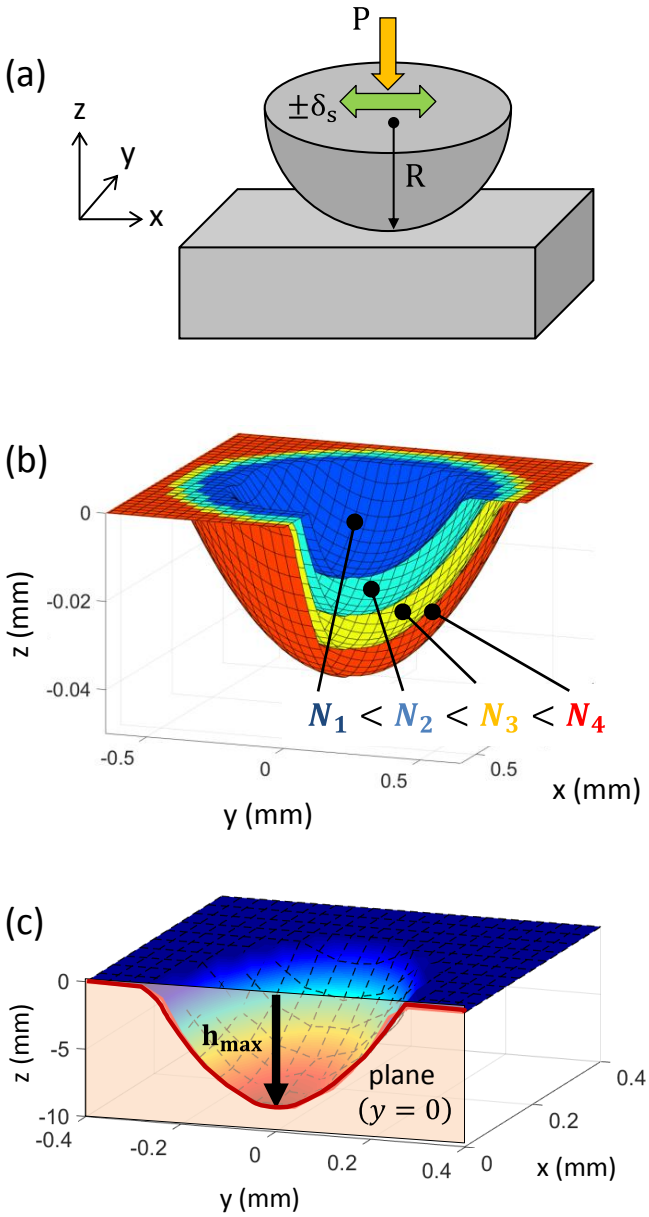


**Fig. 8.** (a) Sphere-on-flat contact configuration description; (b) Evolution of the 3D wear profiles with the number of cycles; (c) Estimation of the maximum wear depth at y=0 in sphere-on-flat contact.

Once again the SA 3D numerical approach is considered as the reference assuming that it provides a precise estimation of the 3D sphere-on-flat pressure profile. Like the 2D cylinder-on-flat contact, the WK model requires the identification of a representative 3D “pressure” stiffness parameter. The strategy proposed by Johnson et al. is still adopted which consists in fitting the WK sphere-on-flat contact radius with the Hertzian value assuming similar contact conditions (i.e. materials, sphere radius and normal load).

### 5.2. Comparison between WK and SA for sphere-on-flat solution

To check the performance of WK approach in 3D configuration, the latter is compared with SA and experimental results for a sphere-on-flat contact [31] whose elastic properties and wear parameters are compiled in Table 3 leading to $p_{0,H}$ = 2235 MPa, $a_H$= 103 µm, K=2.24x10$^6$ MPa/mm.

**Table 3.** Elastic properties and wear parameters used to simulate the experimental results [31] of a sphere-on-flat contact (sphere: Alumina $Al_2O_3$ and plane: HS25).

| Elastic modulus, $E_p$ (GPa) | Poisson’s coefficient, $\nu_p$ | Elastic modulus, $E_c$ (GPa) | Poisson’s coefficient, $\nu_c$ | Wear coef. $\alpha_p$ (mm$^3$/J) | Wear coef. $\alpha_c$ (mm$^3$/J) |
|---|---|---|---|---|---|
| 210 | 0.3 | 310 | 0.25 | 5.3x10$^{-5}$ | 0 |
| Sphere radius, R (mm) | Normal force, P (N) | Sliding amplitude, $\delta_s$ (µm) | Friction coefficient,µ | Number of cycles, N | |
| 4 | 50 | 20 | 0.77 | 200000 cycles | |

#### 5.2.1. Prediction of the maximum wear depth

Fig. 9 shows the evolution of the index error $\%E_{h,WK}$ with respect to the maximum wear depth for the test conditions present in Table 3. The error $\%E_{h,WK}$ decreases significantly from 20% after 200 cycles (i.e. $h_{max}$= 1 µm) to less than 1% after just 4500 cycles (i.e. $h_{max}$= 6 µm). This suggests the efficiency of the WK approach in 3D contact configuration.

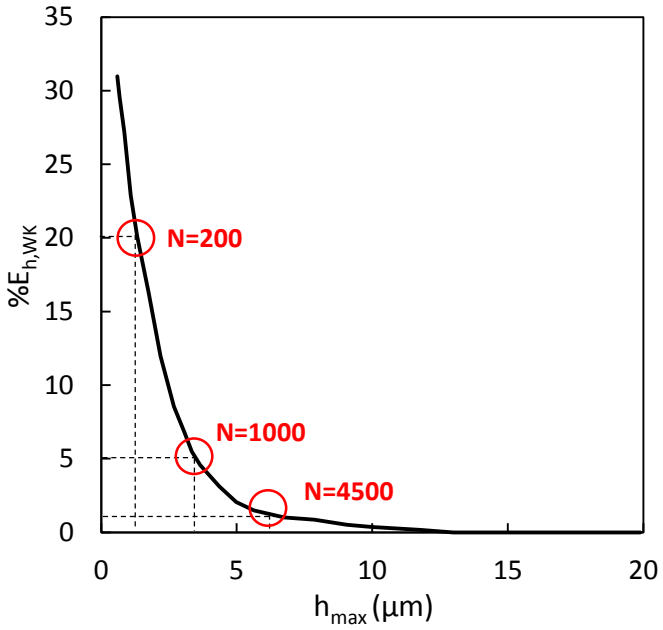


**Fig. 9.** Variation of the error index $\%E_{h,WK}$ with respect to $h_{max}$ for sphere-on-flat contact following the test conditions shown in Table 3.

### 5.2.2. Time computation efficiency

Following the good capacity of wear depth prediction of the WK approach, the time computation efficiency of WK is examined with respect to SA in Fig. 10.

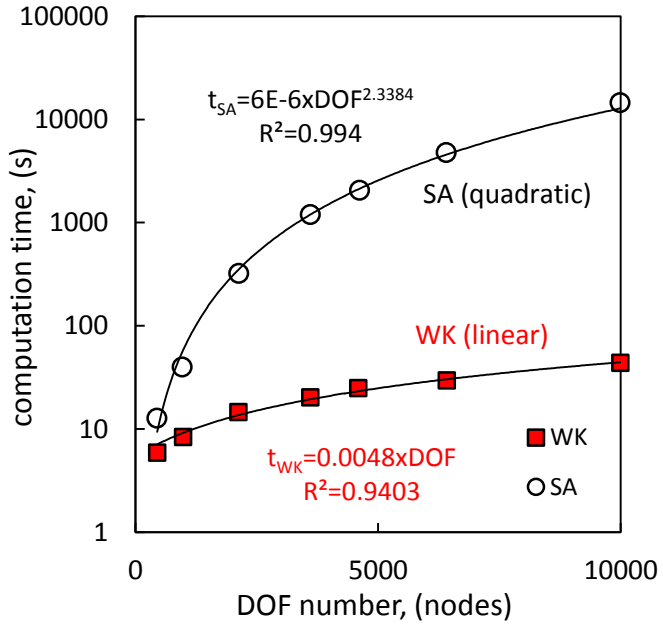


**Fig. 10.** Comparison of the time computation cost with respect to the number of nodes using SA and WK approaches sphere-on-flat contact (Table 3).

Results display a huge reduction of the computational time of the WK approach compared to the SA strategy. Increasing the number of nodes, the computation cost of SA increases quadratically which is not the case of WK where the latter increases linearly suggesting once again that the WK approach provides interesting time computation capacity with respect to SA and surely FEM simulations for 3D surface wear computations.

### 5.2.3. Prediction of the 3D experimental wear profile

After validating the predictive (Fig. 9) and the computational (Fig. 10) efficiency of the WK approach with respect to SA model especially at a large number of fretting cycles, Fig. 11 compares the capacity of the latter to forecast the experimental 3D wear profile applying the experimental conditions shown in Table 3. Results show very nice correlation between experimental and numerical results in both 2D and 3D descriptions of the wear scar which reflects the pertinence of the WK approach in both 2D and 3D Hertzian configurations.

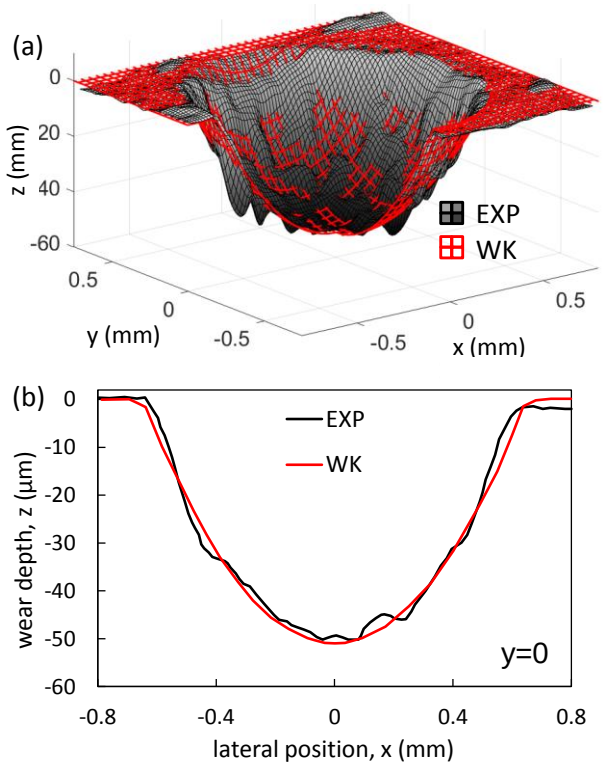


**Fig. 11.** Comparison between the experimental and the numerical (WK) 2D and 3D wear profiles for Hertzian sphere-on-flat contact (Table 3).

## 6. Discussion

The objective of this article is to examine Winkler foundation model to simulate the evolution of wear profile under gross slip fretting loadings in both 2D and 3D Hertzian contacts where both the contact area and the contact pressure evolve with the fretting wear extension. To validate the efficiency of WK approach in predicting wear extension, the latter is compared with semi-analytic and FEM models as well as experiments. As soon as the surface wear depth for the studied condition exceeds few microns, WK approach provides good wear depth estimation very close to that expected by SA and consequently FEM approaches. However, in 2D, the computation efficiency of the WK model is slightly better than the SA model, but much faster than the FEM strategy to model fretting wear. It allows achieving very good wear profile estimations within less than 10 minutes, instead of tens of hours in FEM. In 3D, the WK model seems more efficient than SA model giving access to “simple contact” computations that are already very difficult to obtain with FEM models, due to the heaviness of the latter. More interestingly, such method could be applied to much more complex contacts than the basic Hertzian configurations. Industrial parts could be modeled without applying “geometrical approximations”. It could be also possible to perform geometric optimizations, and parametric studies with short computation times, and without the need to monopolize expensive FEM commercial licenses for weeks. Briefly, the advantage of WK over the two latter approaches is that WK provides lower computations costs. This is quite interesting especially when complex contact configurations are considered where FEM approaches become exhaustive and time consuming. Additionally, WK approach appeared to better predict the wear depth when increasing the sliding amplitude and number of cycles, however, it seemed less efficient when increasing the contact radius or the normal force. This stems from the fact that the latter overestimates the

Hertzian contact pressure and underestimates the contact size leading to fluctuations of the wear depth predictions when changing the normal force and the contact radius. It should be noted that the suggested algorithms of both WK and SA approaches provide reliable wear depth predictions when the fretting contact is not affected by third body particles as the case of interfaces operating in aqueous or lubricated medium. On the hand, the debris layer generated in dry contacts highly affects wear kinetics by affecting the contact pressure distribution and consequently the wear scar evolution as shown recently by Arnaud and co-authors using FEM simulations [23,24]. Additionally, they suggested that the third body layer can be simulated by adding an additional FEM part entrapped between the plane and the counter body. This dynamic simulation allows the third body layer to extend laterally and in thickness depending on the surface wear extension. This can be done by defining a conversion factor "$\gamma_{tb,j}(x)$" which corresponds to the proportion of the worn thickness increment transposed to the third body layer after the $j^{th}$ numerical fretting cycle. Hence, the thickness of the debris layer "$h_{tb,j}(x)$" at the $x$ position and at the $j^{th}$ computation iteration will evolve as follows:

$$h_{tb,j}(x) = h_{tb,j-1}(x) + \gamma_{tb,j}(x) \times (\Delta h_{p,j} + \Delta h_{c,j}) \quad (24)$$

It should be underlined that the complement of the third body transfers (i.e. 1-$\gamma_{tb,j}(x)$) stands for the proportion of the wear particles ejected from the contact. As for wear simulation, similar equations are applied except Eq. 13 & 14 where the presence of the third body is taken into account by replacing $\varphi_{p/c,j}(x)$ by $\varphi_{p/tb,j}(x)$ and $\varphi_{c/p,j}(x)$ by $\varphi_{c/tb,j}$. Here, $\varphi_{p/tb,j}$ is the friction energy density reported on the plane sample due to the friction between the plane and the third body layer (bottom part) and $\varphi_{c/tb,j}$ is the friction energy density reported on the counterpart due to the friction between the latter and the third body (top part). Arnaud et al. [23,24] suggested equally an

approximation of the third body conversion factor "$\gamma_{tb,j}(x)$" using an elliptic function (Eq. 25) of the axial distance (i.e. $x$ abscissa) leading to a maximum value at the contact center.

$$\gamma_{tb,j}(x) = \gamma_0 + K_\gamma \times x^2 \quad (25)$$

The conversion factor parameters were shown [23,24] to depend on the fretting parameters as the number of cycles, contact size and sliding amplitude which affect the retention of the third body particles in the contact and consequently the distribution of the contact pressure and the evolution of the wear profiles. Fig. 12 illustrates the fretting wear scar methodology obtained considering a dynamical evolution of the third body as depicted by Arnaud et al. [23,24].

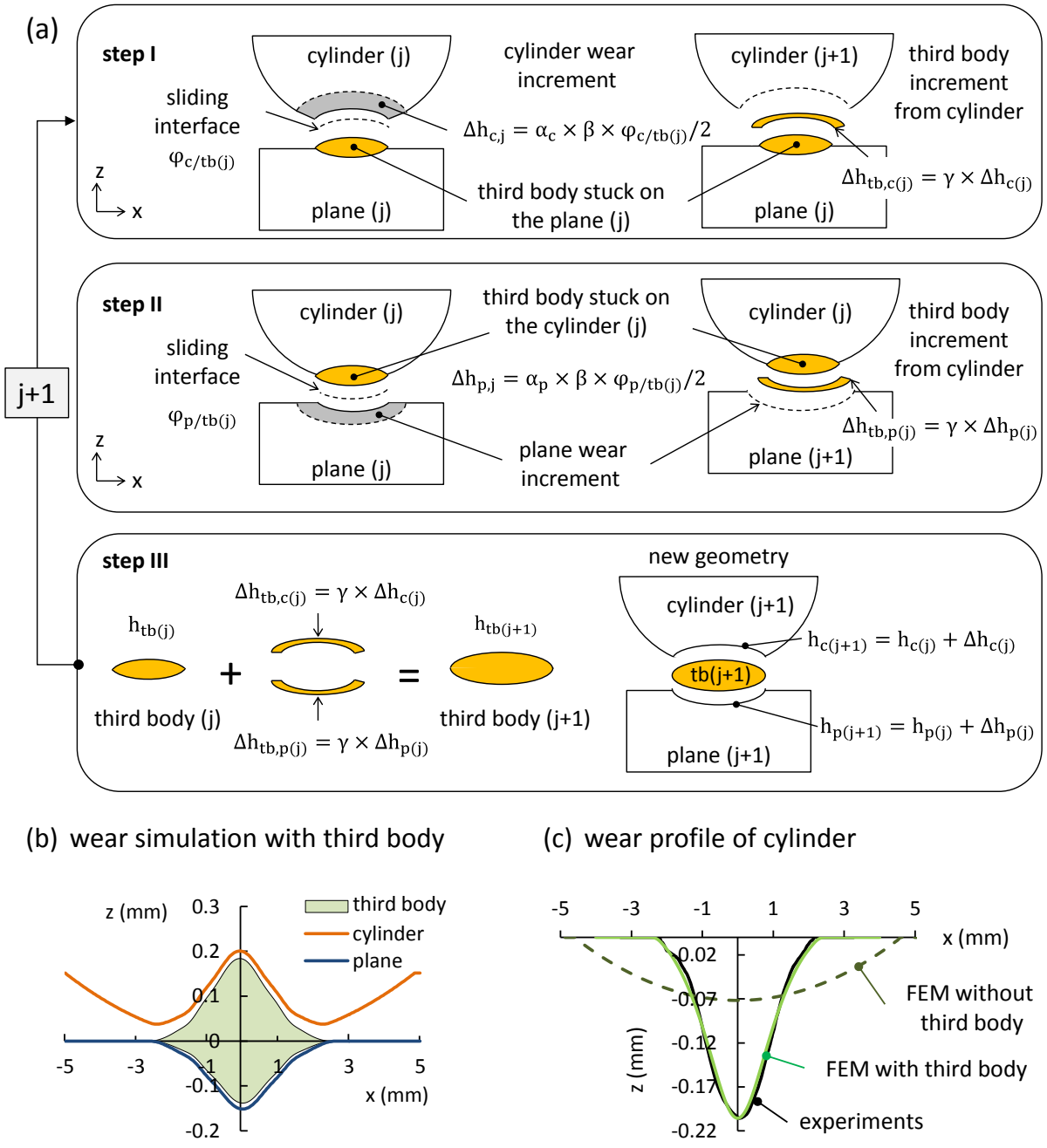


**Fig. 12.** Description of the surface wear modeling based on Arnaud et al. [11,23,24]: (a) illustration of the three-step procedure to update the cylinder and flat surfaces in addition to the third-body layer; (b) illustration of a simulated U-shape fretting scar considering the presence of the third-body layer; (c) comparison between experiments (dry Ti-6Al-4V interface) and simulations with and without simulating the third-body layer (third-body simulation is required to achieve a reliable prediction).

This third body surface wear modeling can be easily integrated in the given WK surface wear simulation. To check the performance of the WK approach, the FEM contact simulation used in [23,24] is replaced here by WK algorithm. Both FEM and

WK simulations are compared to experimental results by using similar Ti-6Al-4V cylinder-on-flat contact conditions where the elastic properties and wear parameters [23,24] are compiled in Table 4 leading to $p_{0,H} = 525$ MPa, $a_H = 1.29$ mm, $K = 0.06 \times 10^6$ MPa/mm.

**Table 4.** Elastic properties and wear parameters used to simulate the experimental results [23,24] of a Ti-6Al-4V cylinder-on-flat contact.

| Elastic modulus, $E_p$ (GPa) | Poisson's coefficient, $\nu_p$ | Elastic modulus, $E_c$ (GPa) | Poisson's coefficient, $\nu_c$ | Wear coef. $\alpha_p$ ($mm^3/J$) | Wear coef. $\alpha_c$ ($mm^3/J$) |
|---|---|---|---|---|---|
| 120 | 0.3 | 120 | 0.3 | $1.6 \times 10^{-4}$ | $2.12 \times 10^{-4}$ |
| Cylinder radius, R (mm) | Normal force, P (N/mm) | Contact pressure $p_{0,H}$ (MPa) | Sliding amplitude, $\delta_s$ (µm) | Friction coefficient, µ | Number of cycles, N |
| 80 | 1066 | 525 | 75 | 0.65 | 10000 |

By considering WK approach to simulate the wear profile evolution instead of the FEM computation both surface wear profiles on the plane and cylinder counterparts can be simulated. Fig. 13 compares both WK and FEM surface wear simulations to experimental wear profiles for the plane and cylinder Ti-6Al-4V specimens with ($\gamma_{tb,j}(x) = \gamma_0 + K_\gamma \times x^2$ with $\gamma_0 = 0.89$ and $K_\gamma = -0.05$) and without ($\gamma = 0$) considering the third body. In all cases, WK wear profiles match perfectly with FEM simulations supporting once again the validity of this approach. However, when the third body is not taken into account, both WK and FEM simulations underestimate the experimental maximum wear depth and overestimate the lateral surface wear extension. This is not the case when third body is introduced in both WK and FEM simulations which correlate perfectly with experimental results.

Such analysis is very interesting as it shows that WK approach predicts well wear profiles in dry contacts involving third body at the interface with remarkably lower computations costs compared to previous FEM simulations.

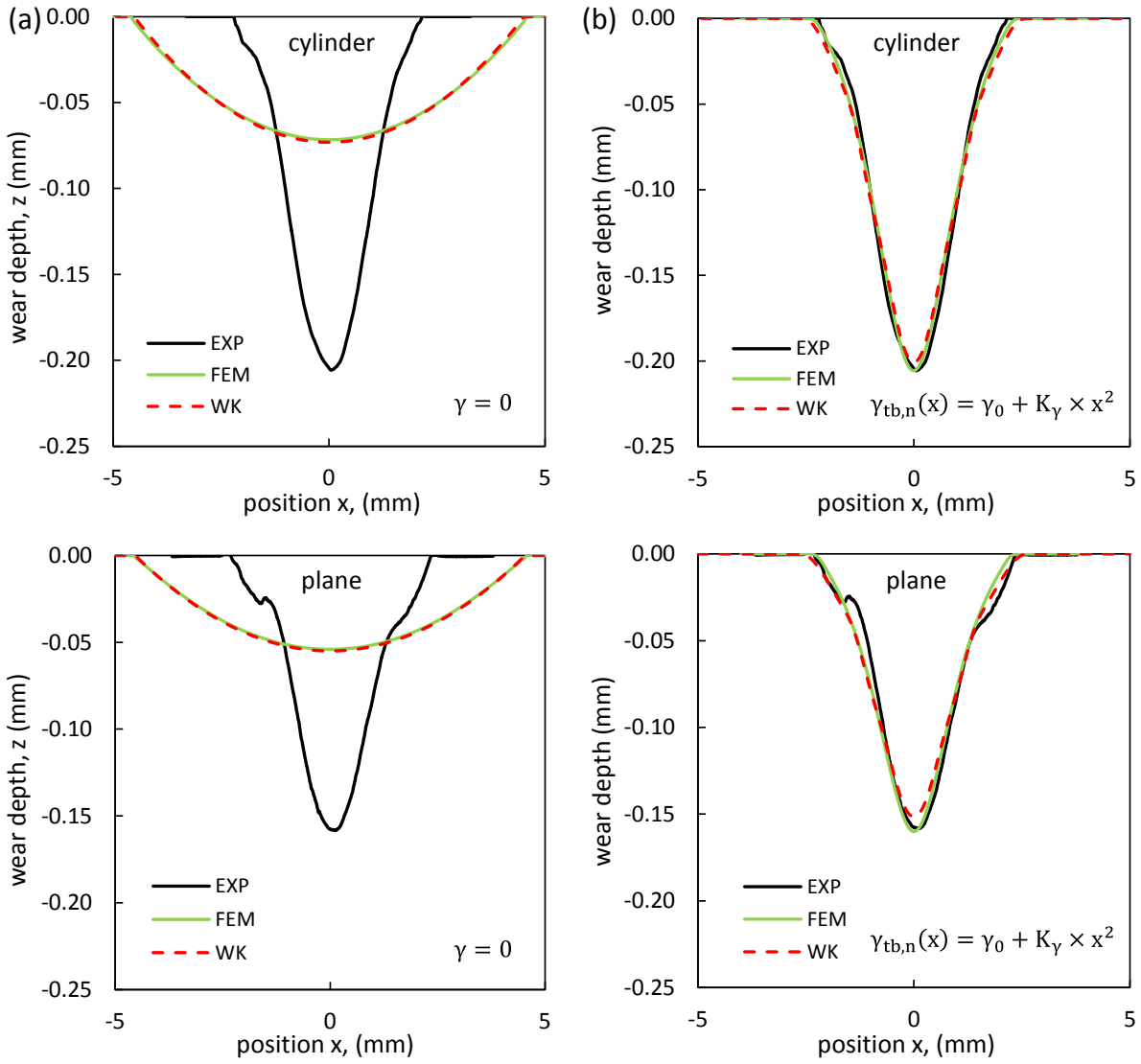


**Fig. 13.** Comparison between the experimental and the simulated plane and cylinder wear profiles of a Ti-6Al-4V interface applying the loading conditions compiled in Table 4: (a) wear simulations without third body consideration (γ = 0) and (b) wear simulations with third body consideration ($\gamma_{tb,n}(x) = \gamma_0 + K_\gamma \times x^2$ with $\gamma_0$ = 0.89 and $K_\gamma$ = −0.05).

The 2D WK approach incorporating third body effect (Fig. 13a) can moreover be transposed to an equivalent 3D sphere-on-flat contact (Fig. 13b) tested under the same conditions shown in Table 4 by applying instead a normal force of P=1100 N leading to $p_{0,H}$ = 525 MPa, $a_H$=1 mm, K=0.11x10$^6$ MPa/mm. This is extremely interesting as it shows that the WK approach can simulate 3D wear profile with debris bed which up to now cannot be investigated using FEM simulations due to the high numerical costs.

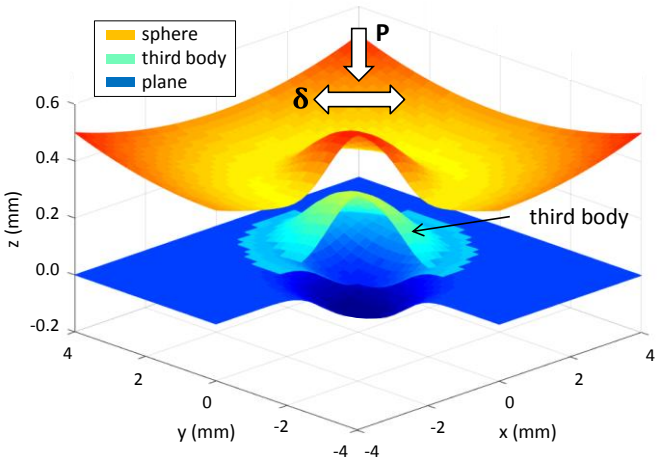


**Fig. 14.** 3D surface wear simulation of a sphere-on-flat Ti-6Al-4V simulation using the WK approach combined with the third body algorithm presented by Arnaud et al. [23] (test conditions in Table 4 leading P=1100 N leading to $p_{0,H} = 525$ MPa with third body consideration such that $\gamma_{tb,n}(x) = \gamma_0 + K_\gamma \times x^2$ with $\gamma_0$ = 0.89 and $K_\gamma$ = −0.05).

The validation of the WK approach compared to FEM and SA numerical strategies for 2D and 3D fretting contacts with and without third body layer suggests that this latter can be applied to simulate much more complex interfaces. Fig. 15a describes the application of WK for a reciprocating sliding for a Hertzian sphere-on-flat contact using the same loading parameters compiled in Table 3 except for $\delta_s$=1 mm and N=5000 cycles. On the other hand, Fig. 15b describes the capacity of WK in simulating unidirectional sliding of a pin-on-disc contact using the same loading parameters shown in Table 3 but with N=20000 cycles. Fig. 16 illustrates the application of the given WK model for an industrial application focusing on the 3D surface wear simulation of a polymer liner involved in the positioning ball assembly of helicopter propeller.

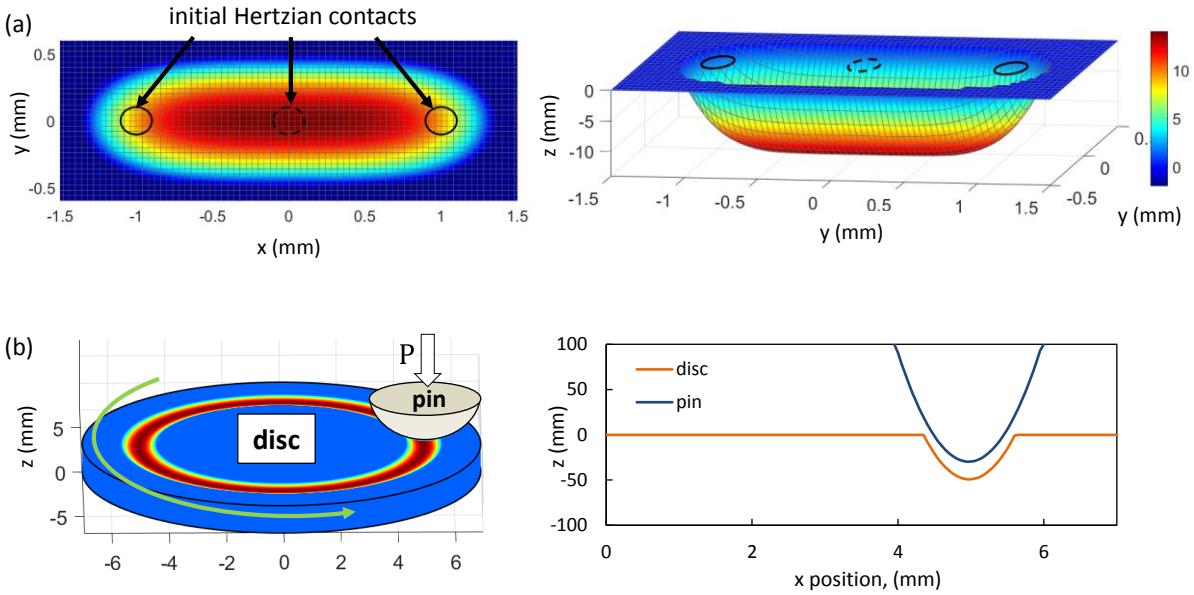


**Fig. 15.** (a) Application of the WK approach for modeling 3D wear profiles for Hertzian sphere-on-flat contacts (Table 3) in the case of (a) reciprocating sliding with $\delta_s$=1 mm and N=5000 cycles, and $\gamma$=0 and (b) unidirectional sliding of a pin-on-disc contact with N=20000 cycles, and $\gamma$=0.

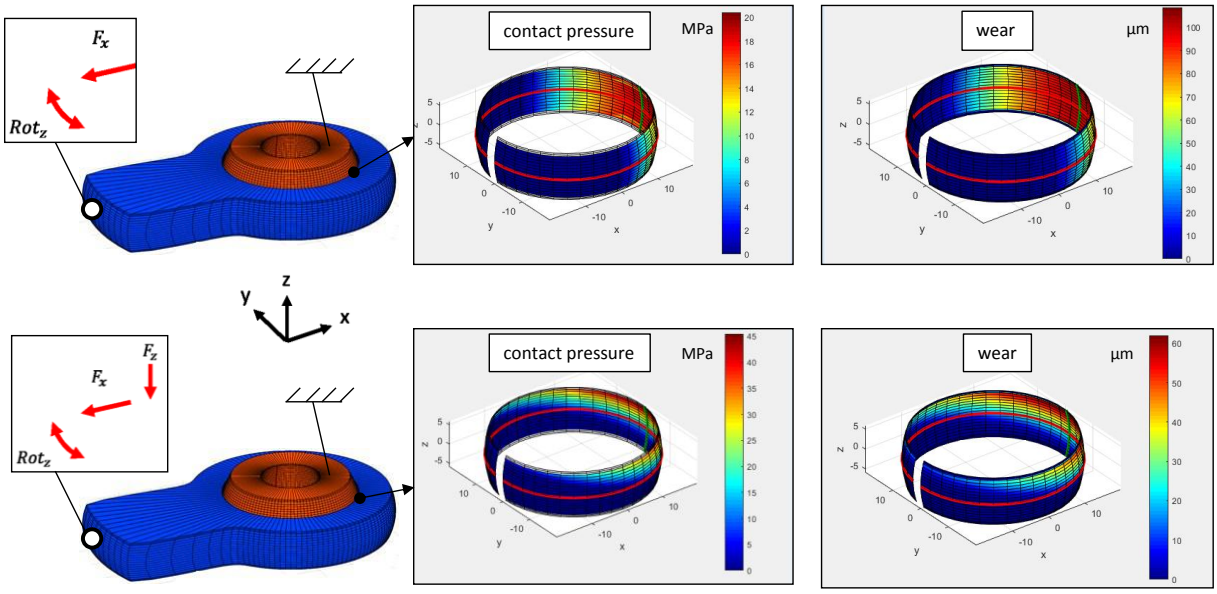


**Fig. 16.** Application of the WK approach for 3D surface wear simulation (without third body consideration) of a polymer liner involved in the positioning ball assembly of helicopter propeller (unfortunately due to confidentiality aspects, the loading conditions as well as the wear rate of the polymer material cannot be detailed).

All these 3D contact configurations are very complex and time consuming using common FEM models but can be easily addressed using the WK contact simulation which seems pertinent to capture 3D surface wear phenomena including the 3D

contact pressure profile evolution in complex industrial applications (Fig. 16). Besides, WK approach appears as a very convenient strategy for going further by modeling the effect of surface roughness, contact geometry and the partition of adhesive and abrasive wear which will be the target of future research.

## 7. Conclusion

The purpose of this study is to model fretting and reciprocating wear in 2D and 3D Hertzian contacts using Winkler elastic foundation model (WK). The main conclusions of this work are the following:

- Although WK approach does not strictly solve the contact interactions and can induce significant wear profile underestimations at the beginning of the surface damage, after few loading cycles, when the wear depth overpasses few microns, the relative errors compared to reference FEM and SA surface wear simulations falls below 5%. The WK strategy appears as a pertinent and fast numerical approach to simulate the steady state wear profile evolutions. The comparison for an equivalent 2D cylinder-on-flat contact shows that WK is 3 times faster than SA and 300 times faster than FEM.
- This very fast numerical strategy allows the simulations of complex 3D contacts which cannot be obtained in a simple way using the conventional FEM method.
- For 3D surface wear simulations, it was shown that if the computation time of SA method evolves to the power 2.3 of the numerical DOF (i.e. number of contact nodes), the computation time required by WK method for similar condition is only proportional to the number of DOF. This confirms the very high efficiency of the WK approach to simulate complex 3D contacts.

- The WK method can successfully be transposed to simulate complex fretting interfaces including the presence of a debris layer for 2D but also 3D fretting contacts
- This approach can be also transposed to longer kinematic sliding conditions like 3D sphere-on-flat reciprocating but also pin-on-disc sliding.

Taking advantage of the fast WK method, future developments will be undertaken to develop 3D multiphysics surface wear simulations like previously developed for 2D cylinder plane contacts [11].

**Acknowledgements**

This research did not receive any specific grant from funding agencies in the public, commercial, or not-for-profit sectors.

**Reference**

[1] J.F. Archard, Contact and rubbing of flat surfaces, J. Appl. Phys. 24 (1953) 981–988. doi:10.1063/1.1721448.
[2] H.C. Meng, K.C. Ludema, Wear models and predictive equations: their form and content, Wear. 181–183 (1995) 443–457. doi:doi:https://doi.org/10.1016/0043-1648(95)90158-2.
[3] S. Fouvry, P. Kapsa, L. Vincent, Quantification of fretting damage, Wear. 200 (1996) 186–205. doi:10.1016/S0043-1648(96)07306-1.
[4] S. Fouvry, P. Kapsa, H. Zahouani, L. Vincent, Wear analysis in fretting of hard coatings through a dissipated energy concept, Wear. 1648 (1997) 393–403.
[5] S. Fouvry, P. Kapsa, An energy description of hard coating wear mechanisms, Surf. Coatings Technol. 138 (2001) 141–148. doi:10.1016/S0257-8972(00)01161-0.
[6] S. Fouvry, P. Duó, P. Perruchaut, A quantitative approach of Ti-6Al-4V fretting damage: Friction, wear and crack nucleation, Wear. 257 (2004) 916–929. doi:10.1016/j.wear.2004.05.011.
[7] J. Ding, I.R. McColl, S.B. Leen, P.H. Shipway, A finite element based approach to simulating the effects of debris on fretting wear, Wear. 263 (2007) 481–491. doi:10.1016/j.wear.2006.12.056.
[8] S. Basseville, E. Héripré, G. Cailletaud, Numerical simulation of the third body in fretting problems, Wear. 270 (2011) 876–887. doi:10.1016/j.wear.2011.02.016.
[9] A. Ghosh, B. Leonard, F. Sadeghi, A stress based damage mechanics model to simulate fretting wear of Hertzian line contact in partial slip, Wear. 307 (2013) 87–99. doi:10.1016/j.wear.2013.08.008.
[10] S. Garcin, S. Fouvry, S. Heredia, A FEM fretting map modeling: Effect of surface wear on crack nucleation, Wear. 330–331 (2015) 145–159. doi:10.1016/j.wear.2015.01.013.
[11] P. Arnaud, S. Baydoun, S. Fouvry, Modeling adhesive and abrasive wear phenomena in fretting interfaces: A multiphysics approach coupling friction energy, third body and contact oxygenation concepts, Tribol. Int. 161 (2021) 107077. doi:10.1016/j.triboint.2021.107077.
[12] B.D. Leonard, A. Ghosh, F. Sadeghi, S. Shinde, M. Mittelbach, Third body modeling in fretting using the combined finite-discrete element method, Int. J. Solids Struct. 51 (2014) 1375–1389. doi:10.1016/j.ijsolstr.2013.12.036.
[13] H. Haddad, M. Guessasma, J. Fortin, A DEM-FEM coupling based approach simulating thermomechanical behaviour of frictional bodies with interface layer, Int. J. Solids Struct. 81 (2016) 203–218. doi:10.1016/j.ijsolstr.2015.11.026.
[14] L. Gallego, D. Nélias, C. Jacq, A comprehensive method to predict wear and to define the optimum geometry of fretting surfaces, J. Tribol. 128 (2006) 476–485. doi:10.1115/1.2194917.

[15] L. Gallego, B. Fulleringer, S. Deyber, D. Nélias, Multiscale computation of fretting wear at the blade/disk interface, Tribol. Int. 43 (2010) 708–718. doi:10.1016/j.triboint.2009.10.011.
[16] Y. Kong, C.J. Bennett, C.J. Hyde, A Computationally Efficient Method for the Prediction of Fretting Wear in Practical Engineering Applications, Tribol. Int. (2021) 107317. doi:10.1016/j.triboint.2021.107317.
[17] P. Põdra, S. Andersson, Wear simulation with the Winkler surface model, Wear. 207 (1997) 79–85. doi:10.1016/S0043-1648(96)07468-6.
[18] K.Y. Choi, S.S. Kim, I.A. Soldatenkov, Modeling of fretting wear based on solution of wear contact problem, Tribol. Lett. 37 (2010) 69–74. doi:10.1007/s11249-009-9491-x.
[19] I.I. Argatov, Y.S. Chai, A self-similar model for fretting wear contact with the third body in gross slip, Wear. 466–467 (2021) 203562. doi:10.1016/j.wear.2020.203562.
[20] K.L. Johnson, Contact mechanics, Cambridge University Press, 1985.
[21] A. Flodin, S. Andersson, Simulation of mild wear in helical gears, Wear. 241 (2000) 123–128. doi:10.1016/S0043-1648(00)00384-7.
[22] T. Telliskivi, U. Olofsson, Wheel-rail wear simulation, Wear. 257 (2004) 1145–1153. doi:10.1016/j.wear.2004.07.017.
[23] P. Arnaud, S. Fouvry, S. Garcin, A numerical simulation of fretting wear profile taking account of the evolution of third body layer, Wear. 376–377 (2017) 1475–1488. doi:10.1016/j.wear.2017.01.063.
[24] P. Arnaud, S. Fouvry, A dynamical FEA fretting wear modeling taking into account the evolution of debris layer, Wear. 412–413 (2018) 92–108. doi:10.1016/j.wear.2018.07.018.
[25] I.I. Argatov, Asymptotic modeling of reciprocating sliding wear with application to local interwire contact, Wear. 271 (2011) 1147–1155. doi:10.1016/j.wear.2011.05.028.
[26] I. Argatov, W. Tato, Asymptotic modeling of reciprocating sliding wear e Comparison with finite-element simulations, Eur. J. Mech. A/Solids. 34 (2012) 1–11. doi:10.1016/j.euromechsol.2011.11.008.
[27] I. Argatov, Y.S. Chai, Contact Geometry Adaptation in Fretting Wear: A Constructive Review, Front. Mech. Eng. 6 (2020) 1–10. doi:10.3389/fmech.2020.00051.
[28] L. Gallego, D. Nélias, S. Deyber, A fast and efficient contact algorithm for fretting problems applied to fretting modes I, II and III, Wear. 268 (2010) 208–222. doi:10.1016/j.wear.2009.07.019.
[29] L. Gallego, D. Nélias, Modeling of fretting wear under gross slip and partial slip conditions, J. Tribol. 129 (2007) 528–535. doi:10.1115/1.2736436.
[30] E. Marc, S. Fouvry, O. Graton, C. Phalippou, H. Maitournam, Fretting wear of a nitrided 316L/304L contact subject to in-phase normal force fluctuation in dry and lithium-boron solution: An RP-friction energy wear approach, Wear. 376–377 (2017) 690–704. doi:10.1016/j.wear.2017.01.075.
[31] A. Dréano, S. Fouvry, G. Guillonneau, A tribo-oxidation abrasive wear model to quantify the wear rate of a cobalt-based alloy subjected to fretting in low-to-medium temperature conditions, Tribol. Int. 125 (2018) 128–140. doi:10.1016/j.triboint.2018.04.032.